IEEE Access
Multidisciplinary | Rapid Review | Open Access Journal

Received January 16, 2020, accepted February 2, 2020, date of publication February 18, 2020, date of current version March 4, 2020.

Digital Object Identifier 10.1109/ACCESS.2020.2974906

Research on a Multi-Motor Coordinated Control Strategy Based on Fuzzy Ring Network Control

YANJUAN WU, YANBIN CHENG, AND YUNLIANG WANG
Tianjin Key Laboratory for Control Theory and Applications in Complicated Systems, Tianjin University of Technology, Tianjin 300384, China
Corresponding author: Yanjuan Wu (wuyanjuan12@126.com)

This work was supported by the Science and Technology Plan Project of Tianjin under Grant 18ZXYENC00100.

ABSTRACT Aiming at the multi-motor coordinated control of intelligent robots, cross-coupling ring control based on fuzzy theory (CRCF) is proposed. Each motor is cross-coupled with two adjacent motors to form a multi-motor ring network structure that eliminates lag in speed tracking between motors and enhances synchronization between motors. Applying fuzzy control to the cross-coupling control of the proposed control strategy, the speed error and change in speed error of two adjacent motors are used as the input of the fuzzy controller, and its output is used as the input of the second of the two adjacent motors. The fuzzy controller achieves real-time tracking adjustment of the speed error between motors. The controllability and observability of the proposed control strategy are verified by the theorem of the Kalman matrix rank criterion. The external stability and internal stability are verified using an impulse response matrix. The theoretical analysis of the lag is verified by establishing a physical and mathematical model. Finally, a four-motor coordination control system model is built. By comparison with the non-ring network proportional cross-coupling control method, the effectiveness of the proposed control strategy is experimentally verified by the MATLAB/Simulink and the RT-LAB real-time simulation platform.

INDEX TERMS Multi-motor coordinated control, ring network control, fuzzy control, stability analysis, lag analysis.

I. INTRODUCTION

In the past 10 years, considerable attention has been paid to artificial intelligence robotic technology, and a large number of repetitive and complex mechanical procedures have gradually been replaced by intelligent robots [1]–[2]. The demand for intelligent robots in various industries is increasing. By performing coordination control, multiple motors can reach higher requirements for tracking, synchronization and position accuracy to drive the robot to achieve similar functions to a human.

To improve synchronization accuracy, early motor coordination control used the load compensation controller method to reduce the asynchronous phenomenon caused by load and torque imbalance [3]. With the continuous development of electronic technology and control theory, some control methods combined with advanced control theory have been used for multi-motor coordination control. High precision and stability are the development trends of multi-motor coordination control. In multi-motor drive industrial production, the stable coordination of the system directly affects the quality of the product. At present, the coordinated control of multi-motor drive systems in industrial production is mainly divided into uncoupled control modes and coupled control modes. Common non-coupling coordinated control methods are the master coordination control method [4] and the master-slave coordinated control method [5], [6]. The disadvantage of non-coupling coordinated control is that the main motor (or main system) does not respond in a timely manner when an external disturbance occurs from the slave motor (or from the slave system). Therefore, there is a lag from slave motor (or slave system) feedback to the main motor (or main system), which affects the synchronicity of the whole multi-motor system.

Koren pioneered the basic structure of a cross-coupled controller on a biaxial motion platform in 1970 [7]. Since then, many scholars have studied the cross-coupling control of two-axis synchronization and two-axis tracking [8]–[10]. The advantages of cross-coupling control in multi-motor coordinated control have been recognized, applied and developed [11]–[18]. Among multi-motor coordinated control strategies, the traditional proportional cross-coupling

The associate editor coordinating the review of this manuscript and approving it for publication was Haipeng Yao.

control strategy (TCCS) has made great progress. However, to achieve more precise motor speed synchronization control and faster and more accurate speed adjustment, the feedback coefficient needs to change continuously with the variation of speed error between adjacent motors. However, the traditional constant feedback coefficient will affect the accuracy and rapidity of synchronous tracking and cause unstable output or even a vibration ripple phenomenon. If the linear change feedback coefficient method is adopted, the feedback coefficient will continue to increase due to the increase in the adjustment time, which will affect the overshoot of the adjustment and may cause the system to oscillate or even collapse.

As one of the important branches of intelligent control, fuzzy control technology has significant advantages for multi-variable complex system with nonlinear, strong coupling, uncertainty and time-varying characteristics. It has been widely used in various control fields and has achieved very effective control effects [19]–[22]. In this paper, considering that the motor is susceptible to different types of disturbances during operation, fuzzy control can be used to distinguish these disturbances according to different fuzzy areas. When the motor is subjected to these disturbances, the speed of each motor can be changed accordingly by the fuzzy control rule. That is, fuzzy control realizes real-time variable coefficient control with disturbance, which improves the coordination of multi-motor operation.

In recent years, with the development of intelligent robot technology and the increasing demand for robot intelligence in the market, multi-motor coordinated control technology has begun to attract more attention. Speed feedback control and torque compensation were used for dual motor coordinated control [23]. The centralized coordinated control (DCC) strategy with multiple subsystems [24], multiple phases motor technology [25], communication topology modules to transmit motor position information [26], the torque distribution method [27]–[32], additional speed controllers [33], the adaptive sliding mode fault-tolerant coordination (ASM-FTC) control method [34], learning adaptive robust control [35] and the hierarchical network method [36] have been used for multi-motor coordinated control.

Although some encouraging progress has been made, developing multi-motor coordinated control with high precision is less successful and still requires further research.

Motivated by the above discussion, this paper proposes a cross-coupling multi-motor ring network control strategy based on fuzzy control rules (CRCF). The main contributions of the proposed control strategy are as follows:

(1) To overcome the shortcomings of master-slave control delay, a ring network control structure is designed to further enhance the coupling and following ability between the motors. In this ring structure, two adjacent motors can be cross-coupled by the controllers, and the first motor and the last motor are also cross-coupled by the controllers. This ring structure can eliminate lag and prevent possible damage to each motor caused by additional mechanical torque due to excessive speed differences.

(2) Fuzzy control is used in cross-coupled controllers to achieve real-time tracking of speed changes between multi-motor. Fuzzy control can change the control parameters of the controller in real time based on speed changes which enhances tracking performance in multi-motor coordinated control. These fuzzy controllers take the speed error of the adjacent motors and its change rate as input and adjust the feedback coefficient according to fuzzy reasoning rules to realize real-time coordinated control between motors which ensures more effectively tracking and coordination between motors.

(3) A method to judge the synchronous performance of motors in the multi-motor coordinated control by the time constant of each motor is proposed, the physical and mathematical models of the method is built, and the concrete derivation method is expounded. By using this method, it is proved that the control strategy proposed in this paper has the advantage of eliminating the lag between motors in the multi-motor coordinated control, which is consistent with the experimental simulation results.

(4) The motion trajectory projection of the manipulator is drawn through the simulation experiment, and the motion trajectory space is illustrated.

This paper is organized as follows: Section 2 consists of the overall ring network structure of the proposed control method and the control principle. Section 3 presents the design of the fuzzy controller and formulates the fuzzy control rules. Section 4 proves the stability of the proposed control strategy. Section 5 analyses the lag problem. Section 6 builds a coordinated control model of four-motor system, and the control effect of the proposed control method is compared with the non-ring network proportional cross-coupling control method by both MATLAB simulation and the RT-LAB real-time experimental platform. Finally, Section 6 summarizes the results of this paper.

II. PROBLEM FORMULATION AND CONTROL METHOD

A. ROBOT STRUCTURE

As shown in Fig. 1, the robot has three arms and one mechanical gripper. The three arms and the mechanical gripper are driven by motors. To ensure that the robot can accurately grasp the target object, these motors must

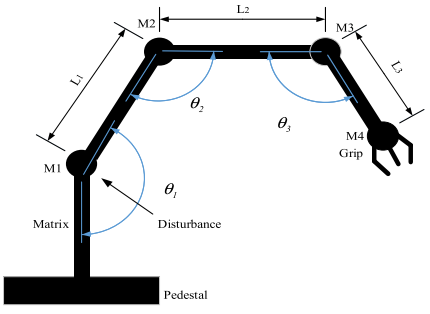

FIGURE 1. The structure diagram of the robot.

coordinate movement. The length and rotation angle of each arm can be obtained by calculation considering arm weight, load weight and target position. When the robot is not disturbed by outside influences, it can accurately grasp the target object. In the absence of coordinated control between motors, if a motor is disturbed, the speed following of other motors is not obvious because the coupling between the motors is not strong. Then, the entire mechanical arm system of the robot will not be able to accurately grasp the target object. At present, the robot manipulator is still in the application stage of directional grasping, which puts large requirements on the working environment because of its weak anti-interference ability. Therefore, to improve the intelligence of the robot manipulator, it is important to study multi-motor coordinated control technology, which enhances the coupling and tracking ability between motors and improves the anti-interference ability. The multi-motor synchronous control algorithms mainly include parallel control, master-slave control and cross-coupling control. The key feature of parallel control is that the control between motors is independent of the motors. That is, if one or several motors are disturbed, the motors will lose synchronization and could even cause the system to collapse. Master-slave control is proposed based on parallel control to improve the coordination of multi-motor control. Under this control strategy, the speed input signal of the slave motor is given by the speed output of the previous motor; therefore, the speed of the slave motor always follows the speed change of its previous motor, which increases the stability of the system to a certain degree. However, if the slave motor is disturbed, the motors prior to the slave motors will not change accordingly, which makes it difficult to eliminate the error generated by the slave motor. When the speed of the slave motor is disturbed, it can not be fed back to change the speed of the prior motors but can only adjust itself and the next motors, which will cause delay. Therefore, master-slave control is unsuitable for high-speed and high-precision applications. The traditional proportional cross-coupling control strategy (TCCS) combines the advantages of parallel control and master-slave control. The speed error of the motors is fed back to their speed input through a constant proportional controller. Thus, each motor can respond to disturbances, but there will still be delay because of the non-ring network structure. At present, most synchronization control algorithms are based on cross-coupling control. However, this control strategy has limitations; it only has a small scope of application in high working environment requirements due to its weak anti-interference ability and response lag. If the synchronization speed error of motors is reduced only by increasing the gain of the controller, the system will be unstable or even collapse. Moreover, because the TCCS is a non-ring network structure, the feedback of speed error between motors will also produce hysteresis, which will cause the control system to not respond in time; thus, the TCCS is unsuitable for occasions with high synchronization precision requirements.

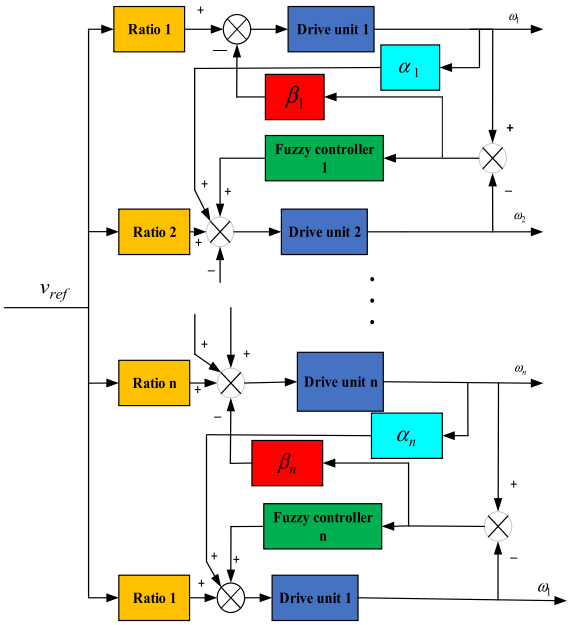

FIGURE 2. The control structure diagram of CRCF.

B. CONTROL METHOD OF CRCF

Due to the difficulties of the TCCS in achieving high-precision synchronous control, CRCF is proposed; it adopts a ring network control structure, and fuzzy control is applied to its cross-coupling control strategy. The control structure diagram of CRCF is shown in Fig. 2.

The improved multi-motor coordinated control strategy combines the advantages of parallel control, master-slave control, cross-coupling control and fuzzy control. It constitutes a ring network control system; that is, each motor is cross-coupled with two adjacent motors to form a multi-motor ring network control structure, which improves speed tracking ability between motors. The proportional coefficient and gain coefficient in Fig. 2 can be adjusted by actual working demand. The fuzzy controller acts as error compensation to eliminate the speed output errors between the motors, which makes the system more coordinated.

III. FUZZY CONTROLLER

A nonlinear fuzzy control algorithm based on fuzzy inference is designed. The input and output selection of the fuzzy controller should be determined according to the actual situation of the control system. The proposed fuzzy controller has two inputs, namely, speed error e and change in speed error ec, and one output c, which is the real time compensation for the change in speed error. e and ec are expressed as follows:

$$\begin{cases} e_i = v_{i(t)} - v_{i+1(t)} \\ ec_i = \dfrac{de_i}{dt} \end{cases} \tag{1}$$

where e_i and ec_i are the output speed error and the change in speed error between the i-th motor and the $(i+1)$-th motor, respectively.

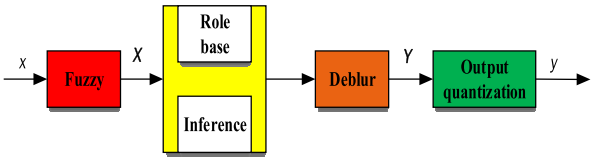

FIGURE 3. Fuzzy principle diagram of the fuzzy controller.

The principle of the fuzzy controller is shown in Fig. 3, which includes fuzzification, a fuzzy rule base, fuzzy inference, defuzzification and output quantization. First, the precise input x is fuzzified into a fuzzy variable $\boldsymbol{X}$; then, the fuzzy rule vector is obtained by referring to the fuzzy inference of the rule base, and subsequently, the fuzzy control variable $\boldsymbol{Y}$ is obtained by deblurring the fuzzy rule vector. Finally, the actual output control quantity y is obtained by output quantization.

A. FUZZY PRINCIPLE

The essence of fuzzification is to map a precise value to a corresponding fuzzy domain. That is, the values input to the fuzzy controller are exact values, and they are blurred by a certain fuzzy logic method. The fuzzy principle includes fuzzy domain mapping, fuzzy domain segmentation, a membership function, and fuzzy output inference.

1) FUZZY DOMAIN MAPPING

The precise input is transformed into a scale value in a fuzzy domain and is mapped to a corresponding fuzzy set. $\Omega_e = (-m, m)$, $\Omega_{ec} = (-n, n)$ and $\Omega_c = (-l, l)$ are, respectively, the fuzzy domain of the input e, the fuzzy domain of the input ec and the fuzzy domain of the output c. k_e and k_{ec}, are, respectively, fuzzy scale factors of the two inputs, which are shown as formulas (2, 3). k_c represents the precise output quantization factor, which is shown as formula (4):

$$k_e = \frac{2m}{e_H - e_L} \tag{2}$$

$$k_{ec} = \frac{2n}{ec_H - ec_L} \tag{3}$$

$$k_c = \frac{c_H - c_L}{2l} \tag{4}$$

where m, n and l correspond to the positive boundary maximum of the corresponding fuzzy domains. e_H, e_L, ec_H, ec_L c_H and c_L are the maximum and minimum values of the inputs and the output estimated through actual engineering experience. Then, the actual input value can be scaled by formula (5) and transformed into the corresponding fuzzy set. The quantization factor of formula (4) is used to calculate the precise output in the subsequent output quantization.

$$F = KX \tag{5}$$

where X $=[e, ec]^{\mathrm{T}}$, K$=[k_e, k_{ec}]^{\mathrm{T}}$, F$=[fe, fec]^{\mathrm{T}}$, $fe \in \Omega_e$, and $fec \in \Omega_{ec}$. fe and fec are scale values that correspond to speed error e and change in speed error ec, respectively. $\boldsymbol{E}$ and $\boldsymbol{EC}$ represent two input fuzzy sets.

TABLE 1. Fuzzy control rule table.

E/C/EC	NB	NM	NS	ZE	PS	PM	PB
NB	NB	NB	NB	NB	NM	ZE	ZE
NM	NB	NB	NB	NB	NS	ZE	ZE
NS	NM	NM	NM	NM	ZE	PS	PS
ZE	NM	NM	NS	ZE	PS	PM	PM
PS	NS	NS	ZE	PS	PM	PM	PM
PB	ZE	ZE	PS	PM	PB	PB	PB
PM	ZE	ZE	PM	PB	PB	PB	PB

2) FUZZY DOMAIN SEGMENTATION

The segmentation of the fuzzy domain needs to define a fuzzy language and a fuzzy rule, and the fuzzy domain is divided into seven fuzzy set intervals according to the fuzzy language: NB (negative big), NM (negative medium), NS (negative small), ZE (zero), PS (positive small), PM (positive medium), PB (positive big). The fuzzy rule reasoning is shown in Table 1.

The fuzzy rule of the fuzzy controller is formulated as follows:

$$\text{IF } (fe \in \boldsymbol{E}_z) \text{ AND } (fec \in \boldsymbol{EC}_j) \text{ THEN } (gc \in \boldsymbol{C}_{zj}).$$

where $\boldsymbol{E}$, $\boldsymbol{EC}$, $\boldsymbol{C}$ = (NB, NM, NS, ZE, PS, PM, PB), and $\boldsymbol{E} \subset \Omega_e$, $\boldsymbol{EC} \subset \Omega_{ec}$, $\boldsymbol{C} \subset \Omega_c$. $1 \le Z \le 7$, $1 \le j \le 7$, $\boldsymbol{E}_z$ and $\boldsymbol{EC}_j$ represent the $z-th$ fuzzy set of $\boldsymbol{E}$ and the $j-th$ fuzzy set of $\boldsymbol{EC}$, respectively. $\boldsymbol{C}_{\mathrm{zj}}$ is the output fuzzy set corresponding to $\boldsymbol{E}_{\mathrm{z}}$ and $\boldsymbol{EC}_{\mathrm{j}}$, which is obtained from Table 1.

When $m = 6$ and $n = 6$, the membership graphs of seven fuzzy sets are shown in Fig. 4.

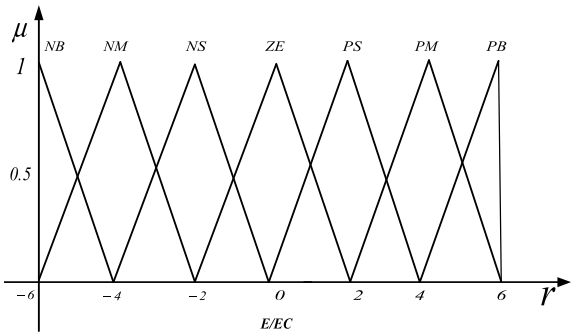

FIGURE 4. Membership function of seven fuzzy sets.

After the scale values of e and ec are calculated by formula (5), their fuzzy sets can be determined from Fig. 4. The fuzzy set of the output is derived from the fuzzy rule above with reference to Table 1. To obtain the output membership that tracks the input changes in real time, the max-min inference algorithm is utilized. The formula of output membership is shown as follows:

$$\mu(C_{zj}) = max\left\lfloor min\{\mu(E_z), \mu(EC_j)\}\right\rfloor \tag{6}$$

B. DEFFUZZIFICATION AND OUTPUT QUANTIZATION

After obtaining the output membership as described above, the centre of gravity method is used to calculate the scale

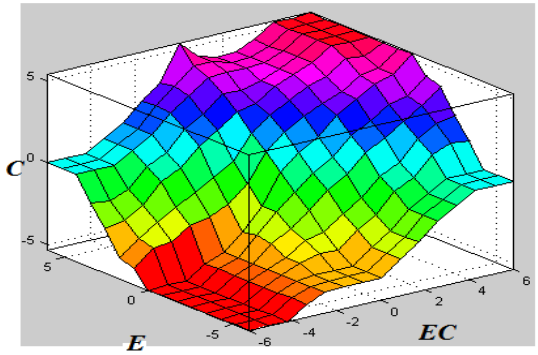

FIGURE 5. The relationship surface of the fuzzy inputs and output.

value of the output, as shown in formula (7).

$$y_{(z,j)} = \frac{\int_a^b \mu(c_{zj}) c_{zj} dc_{zj}}{\int_a^b \mu(c_{zj}) dc_{zj}} \tag{7}$$

where $y_{(z,j)}$ is the scale value of the output corresponding to the two inputs e and ec. Because the centre of gravity method has smoother output inference control, when the input signal changes slightly, the output value on the basis of the above fuzzy inference will also change. It can accurately track changes. The relationship surface of the fuzzy inputs and output is shown in Fig. 5.

Combining the scale value of formula (7) and the quantization factor of formula (4), the feedback output value $y_{f(i)}$ of the fuzzy controller can be formulated as follows:

$$y_{f(i)} = k_c \times y(z, j) \tag{8}$$

where $y_{f(i)}$ is the $(i+1)-th$ motor input. The output result of the fuzzy controller is transmitted to the next motor in the form of speed compensation to achieve speed tracking adjustment.

When the motors run without disturbance, the fuzzy controllers do not work. CRCF is the same as the proportional cross-coupling ring network control. When a motor is subjected to external disturbances during normal running, speed errors will occur, and the fuzzy controllers will output the corresponding feedback coefficients to the speed error, which makes the control method more applicable and flexible. The core of the control strategy is the fuzzy controller. It adjusts the feedback coefficient of the fuzzy controller with the speed error in real time to keep multi-motor running synchronously at specific speeds. This method can be applied to a wider speed range. Moreover, good speed following ability can be achieved in the case of multiple disturbances.

IV. STABILITY ANALYSIS

It can be seen from Fig. 2 that the input of each motor includes four parts: the master-slave feedback input of the upper motor, the rated input, the fuzzy feedback input and the backward feedback input of the next motor.

$$\begin{bmatrix} v_1 \\ v_2 \\ \vdots \\ v_i \\ \vdots \\ v_n \end{bmatrix} = \begin{bmatrix} v_{ref\,1} \\ v_{ref\,2} \\ \vdots \\ v_i \\ \vdots \\ v_{refn} \end{bmatrix} + \lambda A \begin{bmatrix} \omega_{n(t)} \\ \omega_{1(t)} \\ \vdots \\ \omega_{i-1(t)} \\ \vdots \\ \omega_{n-1(t)} \end{bmatrix} + \lambda B \begin{bmatrix} \Delta\omega_{1(t)} \\ \Delta\omega_{2(t)} \\ \vdots \\ \Delta\omega_{i(t)} \\ \vdots \\ \Delta\omega_{n(t)} \end{bmatrix} + \lambda \begin{bmatrix} y_{fn(t)} \\ y_{f\,1(t)} \\ \vdots \\ y_{fi-1(t)} \\ \vdots \\ y_{fn-1(t)} \end{bmatrix} \tag{9}$$

where $A = diag(\alpha_n, \alpha_1, \alpha 2, \alpha_3, \cdots, \alpha_i, \cdots, \alpha_{n-1},)$, $B = diag(\beta_1, \beta_2, \beta_3, \cdots \beta_i, \cdots \beta n)$ α is the master-slave feedback coefficient, β is the backward feedback coefficient, λ is the conversion coefficient between velocity and angular velocity, ω is the motor output angular velocity, $\Delta\omega_i$ is the angular velocity difference between the *i-th* and *(i+1)-th* motors, n is the motor number, v_i is the input speed for the *i-th* motor, and the system rated input is v_{refi}. The master-slave feedback input of the *i-th* motor comes from the previous motor, and its value is $\lambda\alpha_{i-1}\omega_{i-1}$. The backward feedback input of the *i-th* motor is $\lambda\beta_i\omega_i$. The fuzzy feedback input of the *i-th* motor is $\lambda y_{f(i-1)}$.

To simplify the AC asynchronous motor vector control, the following assumptions are made:

1) We ignore the iron loss of the asynchronous motor.

2) We ignore the influence of the small rotating electromotive force of the asynchronous motor and nonlinear coupling caused by the rotating electromotive force.

3) We assume that each link is linear.

4) The rotor flux is considered to be constant in dynamic conditions.

Then, the vector control structure block diagram of the *i-th* asynchronous motor is shown in Fig. 6.

When the load disturbance is zero, the open-loop transfer function of the closed-loop system can be simplified as shown in Fig. 7.

According to the engineering requirement, the typical type II system is used, and the open loop gain can be obtained from Fig. 7.

$$K_N = \frac{P_N K_S K_T K_n}{\lambda J_D R} = \frac{h+1}{2h^2 T_l^2} \tag{10}$$

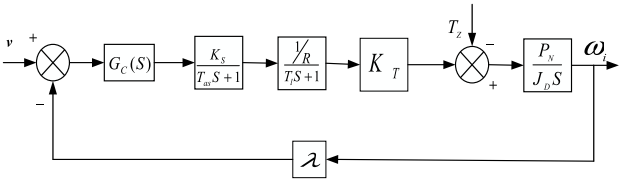

FIGURE 6. The vector control diagram of the *i-th* motor.

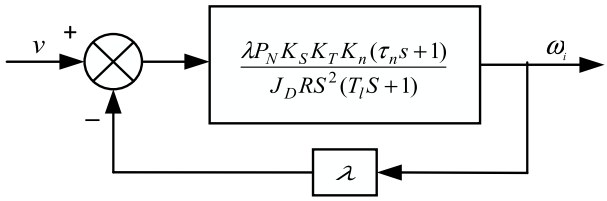

FIGURE 7. The simplified vector control structure of the *i-th* motor.

$$\tau_n = hT_l \tag{11}$$

where h is the width of the Bode diagram when the slope is -*20 dB/dec*. Taking h =5:

$$K_n = \frac{\lambda J_D R K_N}{P_N K_S K_T} \tag{12}$$

where T_{as} is the delay time of the main circuit receiving the control signal (generally ignored in engineering applications), K_s is the amplification factor of the control signal for the main circuit switch, R is motor phase resistance, T_l is the electromagnetic time constant, K_T is the transfer coefficient from torque current to torque, P_N is the number of motor pole pairs, J_D is the motor moment of inertia, which represents the angular velocity, and $G_C(2)$ is equal to $K_n(\tau_n S + 1)/S$. The closed-loop transfer function of the AC asynchronous motor drive unit vector control system is as follows:

$$\begin{aligned} G(2) = \frac{\omega}{V} &= \frac{(P_N R + J_D R K_N \tau_n)S + J_D R K_N / \lambda}{J_D R T_l S^3 + J_D R S^2 + J_D R K_N \tau_n S + J_D R K_N} \\ &= \frac{b_1 S + b_0}{S^3 + a_2 S^2 + a_1 S + a_0} \end{aligned} \tag{13}$$

where $b_1 = \frac{P_N R + J_D R K_N \tau_n}{J_D R T_l}$, $b_0 = \frac{J_D R K_N / \lambda}{J_D R T_l}$, $a_2 = \frac{1}{T_l}$, $a_1 = \frac{K_N \tau_n}{T_l}$, $a_0 = \frac{J_D R K_N}{J_D R T_l}$. The high-order differential formula deduced by formula (13) is shown in formula (14).

$$\omega^{(3)} + a_2\omega^{(2)} + a_1\omega^{(1)} + a_0\omega = b_1 v^{(1)} + b_0 v \tag{14}$$

Introducing the differential operator $p = d/dt$, formula (13) can be expressed as:

$$y = \frac{b_1 p + b_0}{p^3 + a_2 p^2 + a_1 p + a_0} u \tag{15}$$

which can also be expressed as:

$$\begin{cases} \tilde{y} = \dfrac{u}{p^3 + a_2 p^2 + a_1 p + a_0} \\ y = (b_1 p + b_0)\tilde{y} \end{cases} \tag{16}$$

and

$$\begin{cases} \tilde{y}^{(3)} + a_2\tilde{y}^{(2)} + a_1\tilde{y}^{(1)} + a_0\tilde{y} = u \\ y = b_1\tilde{y}^{(1)} + b_0\tilde{y} \end{cases} \tag{17}$$

Then, the system is known to be 3rd order; therefore, there are 3 state variables, which are taken as $x_1 = \tilde{y}, x_2 = \tilde{y}^{(1)}$ and $x_3 = \tilde{y}^{(2)}$.

$$\begin{cases} \dot{x}_1 = \tilde{y}^{(1)} = x_2 \\ \dot{x}_2 = \tilde{y}^{(2)} = x_3 \\ \dot{x}_3 = -a_0 x_1 - a_2 x_2 - a_2 x_3 + u \\ y = b_0 x_1 + b_1 x_2 \end{cases} \tag{18}$$

where $x = [x_1, x_2, x_3]^{\mathrm{T}}$ represents the state vector. The state variable formula in matrix form is shown in formula (19):

$$\begin{cases} \dot{x} = Ax + Bu \\ y = Cx \end{cases} \tag{19}$$

The expanded formula is shown as formula (20).

$$\begin{aligned} \dot{x} &= \begin{bmatrix} 0 & 1 & 0 \\ 0 & 0 & 1 \\ -a_0 & -a_1 & -a_2 \end{bmatrix} x + \begin{bmatrix} 0 \\ 0 \\ 1 \end{bmatrix} u \\ y &= [b_0, \quad b_1, \quad 0] \begin{bmatrix} x_1 \\ x_2 \\ x_3 \end{bmatrix} \end{aligned} \tag{20}$$

where $y = \omega$.

Definitions: The complete controllability of the system: Each state variable within the system can be fully affected by the input. The complete observability of the system: The output can fully react to each state variable within the system.

The controllability of the system is demonstrated by using the Kalman rank criterion. For continuous time-invariant systems, the controllable criterion matrix is constructed by formula (19):

$$Qc = \begin{bmatrix} B & AB & \cdots & A^{n-1}B \end{bmatrix} \tag{21}$$

The necessary and sufficient condition for system stability must satisfy the following formula:

$$rank(Qc) = \begin{bmatrix} B & AB & \cdots & A^{n-1}B \end{bmatrix} = n \tag{22}$$

Proof: Assuming the system is not completely controllable, the Gram matrix is a singular matrix given as follows:

$$W_c \begin{bmatrix} 0, & t_1 \end{bmatrix} = \int_0^{t_1} e^{-At} B B^T e^{-A^T t} dt, \quad \forall t_1 > 0 \tag{23}$$

This demonstrates that there is at least one nonzero state in the state space $\mathscr{R}^{\mathrm{nn}}$, which means the following formula established.

$$\begin{aligned} 0 = \alpha^T W_c \begin{bmatrix} 0, & t_1 \end{bmatrix} \alpha &= \int_0^{t_1} \alpha^T e^{-At} B B^T e^{-AT_t} \alpha dt \\ &= \int_0^{t_1} \left[\alpha^T e^{-At} B\right] \left[\alpha^T e^{-At} B\right]^T dt \end{aligned} \tag{24}$$

Then, $\alpha^T e^{-At} B = 0, \forall t \in \begin{bmatrix} 0, & t_1 \end{bmatrix}$. Deriving the variable t of the above formula (*n-1*) times, let *t=0*; the derived results are $\alpha^T B = 0, \alpha^T AB = 0, \alpha^T A^2 B = 0, \ldots, \alpha^T A^{n-1} B = 0$. The formula can be expressed as formula (25).

$$\alpha^T \begin{bmatrix} B & AB & \cdots & A^{n-1}B \end{bmatrix} = \alpha^T Q_c = 0 \tag{25}$$

Due to $\alpha \neq 0$, Q_c is linearly correlated, that is, rank$(Q_c) < n$, which contradicts rank $(Q_c) = n$. Therefore, the system is completely controllable, and the sufficiency is proven.

Proof: Assuming rank $(Q_c) < n$ is a linear correlation, there is at least one nonzero state in the state space R^n, which means the following formula is established.

$$\alpha^T Q_c = \alpha^T \begin{bmatrix} B & AB & \cdots & A^{n-1}B \end{bmatrix} = 0 \tag{26}$$

Therefore, it can be derived as $\alpha^T A^p B = 0$, *P=0,1,2,..., n-1*. Then, for any $t_1>0$, the conclusion can be obtained that $\pm\alpha^T \frac{A^p t^p}{p!} = 0, \forall t \in [0, t_1]$, *P=0,1,2,....* Therefore, based on this conclusion, $0 = \alpha^T \int_0^{t_1} e^{-At} B B^T e^{-AT_t} dt\alpha = \alpha^T W_c [0, t_1] \alpha$ can be inferred. This finding means that the Hermitian matrix $W_c [0, t_1]$ is singular; therefore, the system is not fully controllable, which contradicts the hypothesis. Then, rank $(Q_c) = n$ has been proven.

According to formula (19,20), the matrix is obtained as

$$AB = \begin{bmatrix} 0 \\ 1 \\ -a_2 \end{bmatrix}, \quad \begin{bmatrix} B, & AB, & A^2B \end{bmatrix} = \begin{bmatrix} 0 & 0 & 1 \\ 0 & 1 & -a_2 \\ 1 & -a_2 & a_2^2 - a_1 \end{bmatrix}$$

Then, $rank(Qc) = Rank(B, AB, A^2B) = 3$, which meets the Kalman rank criterion; therefore, the system is completely controllable.

The observability of the system is proven by using the rank criterion. For a continuous, time invariant system, the rank criterion matrix is constructed by formulas (19, 20), and the discriminant matrix is as follows:

$$Q_\circ = \begin{bmatrix} C \\ CA \\ \vdots \\ CA^{n-1} \end{bmatrix} \tag{27}$$

The necessary and sufficient condition for the complete observability of the system must satisfy the following formula:

$$rank(Q_\circ) = rank \begin{bmatrix} C \\ CA \\ \vdots \\ CA^{n-1} \end{bmatrix} = n \tag{28}$$

According to formulas (19, 20), the expressions of matrix C, CA, CA^2 are $C = [b_0 \ b_1 \ 0]$, and $CA = [0 \ b_0 \ b_1]$, and $CA^2 = [-b_1 a_0 \ -b_1 a_1 \ b_0 - b_1 a_2]$. Then,

$$rank(Q_\circ) = rank \begin{bmatrix} b_0 & b_1 & 0 \\ 0 & b_0 & b_1 \\ -b_1 a_0 & -b_1 a_1 & b_0 - b_1 a_2 \end{bmatrix} = n \tag{29}$$

which meets the rank criterion. Therefore, the system is completely observable.

For the time-invariant system analysis, the expression of the relationship of the impulse response matrix is $H(t) = Ce^{At}B$. According to formulas (19,20),

$$A = \begin{bmatrix} 0 & 1 & 0 \\ 0 & 0 & 1 \\ -a_0 & -a_1 & -a_2 \end{bmatrix}, e^{At} = P \begin{bmatrix} e^{\lambda_1 t} & & \\ & e^{\lambda_2 t} & \\ & & e^{\lambda_3 t} \end{bmatrix} P^{-1},$$

where $\lambda_1, \lambda_2, \lambda_3$ are the eigenvalues of A, P represents the eigenvector matrix and p^{-1} represents the eigenvector inverse matrix. Then, the impulse response matrix is obtained.

$$H(t) = [b_0 \ \ b_1 \ \ 0] P \begin{bmatrix} e^{\lambda_1 t} & & \\ & e^{\lambda_2 t} & \\ & & e^{\lambda_3 t} \end{bmatrix} P^{-1} \begin{bmatrix} 0 \\ 0 \\ 1 \end{bmatrix} \tag{30}$$

When all elements of the impulse response matrix satisfy $\int_0^\infty |h(t)|dt < \infty$, the system has external stability.

V. ANALYSIS OF LAG PROBLEMS

The lag problem is one of the key problems to be solved in multi-motor coordinated control. It reflects the coordination and following ability of multi-motor after disturbance. The lag problem can be analyzed by deriving the response time constant of each motor using an equivalent circuit [37], [38]. The response time constant of each motor using the CRCF method and TCCS method are derived as follows. The speed control uses a variable frequency speed controller with vector control. According to the assumptions made in the mathematical model of the asynchronous motor, the A, B, and C three-phase stationary coordinate system is transformed to the $\alpha\beta$ stationary coordinate system, which is shown in Fig. 8.

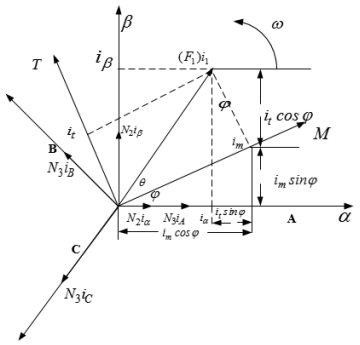

FIGURE 8. The vector diagram of the motor coordinate transformation.

where N_3 is the effective number of turns of each phase in the three-phase winding, and N_2 is the effective number of turns of each phase in the two-phase winding. The coordinate transformation can be written in matrix form as follows.

$$\begin{bmatrix} i_\alpha \\ i_\beta \end{bmatrix} = \frac{N_3}{N_2} \begin{bmatrix} 1 & -\frac{1}{2} & -\frac{1}{2} \\ 0 & \frac{\sqrt{3}}{2} & -\frac{\sqrt{3}}{2} \end{bmatrix} \begin{bmatrix} i_A \\ i_B \\ i_C \end{bmatrix} \tag{31}$$

Under the premise that the total power before and after the conversion is unchanged, it can be proved that the turns ratio should be: $\frac{N_3}{N_2} = \sqrt{\frac{2}{3}}$.

Therefore, it is defined as a transformation matrix $C_{3/2}$ transformed from a three-phase coordinate system to a two-phase coordinate system.

Then

$$C_{3/2} = \sqrt{\frac{2}{3}} \begin{bmatrix} 1 & -\frac{1}{2} & -\frac{1}{2} \\ 0 & \frac{\sqrt{3}}{2} & -\frac{\sqrt{3}}{2} \end{bmatrix} \tag{32}$$

The transformation from the stationary coordinate system $\alpha\beta$ to the two-phase rotational coordinate system MT is a Park transformation. Let the two-phase AC currents i_α and i_β produce the same combined magnetic force as the two-phase DC currents i_m and i_t at a speed of ω_1. Because the $\alpha\beta$ coordinates are stationary in Fig. 8, the MT axis and the vector $(F_1)i_1$ rotate at speed ω_1, and i_m and i_t are unchanged. However, the angle φ between the α-axis and the M-axis changes with time; therefore, the lengths of i_α and i_β on the $\alpha\beta$ axis also change with time. The relationship is as follows:

$$i_\alpha = i_m \cos\varphi - i_t \sin\varphi \tag{33}$$

$$i_\beta = i_m \sin\varphi + i_t \cos\varphi \tag{34}$$

Therefore,

$$C_{2r/2s} = \begin{bmatrix} \cos\varphi & -\sin\varphi \\ \sin\varphi & \cos\varphi \end{bmatrix} \tag{35}$$

Using the above coordinate transformation, the voltage equation of the AC asynchronous motor on the MT coordinate system can be obtained as follows:

$$\begin{bmatrix} u_{sM} \\ u_{sT} \\ u_{rM} \\ u_{rT} \end{bmatrix} = \begin{bmatrix} R_s + pL_s & -\omega_{s1}L_s & pL_m & -\omega_{s1}L_m \\ -\omega_{s1}L_s & R_s + pL_s & -\omega_{s1}L_s & pL_m \\ pL_m & 0 & R_r + pL_r & 0 \\ -\omega_{s1}L_s & 0 & -\omega_{s1}L_s & R_r \end{bmatrix} \times \begin{bmatrix} i_{sM} \\ i_{sT} \\ i_{rM} \\ i_{rT} \end{bmatrix} \tag{36}$$

The flux linkage equation of the AC asynchronous motor in the MT coordinate system is as follows:

$$\begin{bmatrix} \varphi_{sM} \\ \varphi_{sT} \\ \varphi_{rM} \\ \varphi_{rT} \end{bmatrix} = \begin{bmatrix} L_s & 0 & L_m & 0 \\ 0 & L_s & 0 & L_m \\ L_m & 0 & L_r & 0 \\ 0 & L_m & 0 & L_r \end{bmatrix} \begin{bmatrix} i_{sM} \\ i_{sT} \\ i_{rM} \\ i_{rT} \end{bmatrix} \tag{37}$$

The electromagnetic torque is:

$$T_e = \frac{3}{2} P_N L_m (i_{sT} i_{rM} - i_{sM} i_{rT}) \tag{38}$$

where u_{sM} and u_{sT} are the stator voltage on the MT axis. u_{rM} and u_{rT} are rotor voltages on the MT axis. i_{sM} and i_{sT} are the stator currents on the MT axis. i_{rM} and i_{rT} are rotor currents on the MT axis. φ_{sM} and φ_{sT} are stator flux linkages on the MT shaft. φ_{rM} and φ_{rT} are rotor flux linkages on the MT shaft. P_N is the number of pole pairs. L_s, L_r and L_m are the stator inductance, rotor inductance and mutual inductance, respectively. R_s and R_r are the stator and rotor resistance, respectively. ω_{s1} is the stator synchronous angular velocity. ω_s is the slip angular velocity, and $\omega_s = \eta\omega_{s1} = \omega_{s1} - \omega_r$. η is the slip rate. ω_r is the angular velocity of the rotor. φ_r is the rotor flux linkage which rotates at a synchronous speed; therefore, $\varphi_{rM} = \varphi_r$ and $\varphi_{rT} = 0$. The flux linkage can be derived as follows:

$$\begin{bmatrix} \varphi_{sM} \\ \varphi_{sT} \\ \varphi_{rM} \\ 0 \end{bmatrix} = \begin{bmatrix} L_s & 0 & L_m & 0 \\ 0 & L_s & 0 & L_m \\ L_m & 0 & L_r & 0 \\ 0 & L_m & 0 & L_r \end{bmatrix} \begin{bmatrix} i_{sM} \\ i_{sT} \\ i_{rM} \\ i_{rT} \end{bmatrix} \tag{39}$$

For squirrel -cage AC motors, the voltage equation can be derived as follows.

$$\begin{bmatrix} u_{sM} \\ u_{sT} \\ 0 \\ 0 \end{bmatrix} = \begin{bmatrix} Rs + pL_s & -\omega_{S1}L_s & pL_m & -\omega_{S1}L_m \\ \omega_{S1}L_s & R_s + pL_s & \omega_{S1}L_m & pL_m \\ pL_m & 0 & R_r + pL_r & 0 \\ \omega_S L_m & 0 & \omega_S L_r & R_r \end{bmatrix} \times \begin{bmatrix} i_{sM} \\ i_{sT} \\ i_{rM} \\ i_{rT} \end{bmatrix} \tag{40}$$

The flux linkage of the rotor can be obtained from formula (39):

$$\varphi_r = \varphi_{rM} = L_m i_{sM} + L_r i_{rM} \tag{41}$$

The current i_{sM} can be obtained from formula (40):

$$i_{rM} = -p\frac{\varphi_r}{R_r} \tag{42}$$

Substituting formula (42) into the formula (41), we obtain

$$\varphi_r = \frac{i_{sM} L_m}{1 + \frac{L_r}{R_r} p} \tag{43}$$

$$T_e = \frac{3}{2} P_N \frac{L_m}{L_r} i_{sT} \varphi_r \tag{44}$$

Then, $T_r = \frac{L_r}{R_r}$.

Considering iron loss and leakage reactance, and normalizing the stator side to the rotor side, the equivalent circuit of the asynchronous motor can be obtained as shown in Fig. 9.

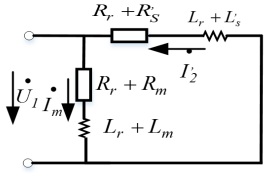

FIGURE 9. The equivalent circuit of a single motor.

where R_s' and L_s' are the equivalent resistance and the equivalent reactance, respectively, calculated from the stator side to the rotor side. R_m and L_m are the iron loss resistance and leakage resistance, respectively. Because $L_m \gg L_r$, the equivalent circuit is as shown in Fig. 10, after ignoring iron loss and leakage reactance.

The time constant of a single motor is obtained as follows:

$$T = \frac{L_r + L_S'}{R_r + R_S'}$$

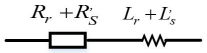

FIGURE 10. The simplified equivalent circuit of a single motor.

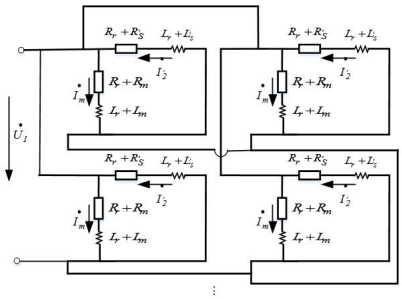

FIGURE 11. The equivalent circuit of multiple motors using CRCF.

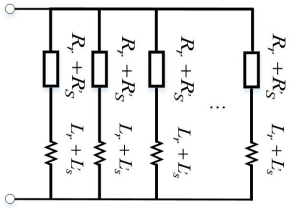

FIGURE 12. The simplified equivalent circuit of multiple motors using CRCF.

In the case of multi-motor control using TCCS control, the equivalent circuit between the motors is connected in series. When a motor is disturbed, the disturbance signal must be transmitted step by step; furthermore, the further the distance from a motor to the disturbed motor, the longer the response time of the motor. For example, when the No.1 motor is disturbed, the response time of the No.4 motor should be 4 times as much as that of the No. 1 motor. That is, $T_1 = T$, $T_4 = 4T$.

When using the CRCF method, due to its multi-motor ring network control structure, the equivalent circuit diagram is as shown in Fig. 11.

The equivalent circuit after ignoring the leakage reactance is shown in Fig. 12.

When n motors form a control ring network in Fig.13, the equivalent resistance is $R_{eq} = \frac{1}{n}(R_r + R_s')$, and the equivalent inductance is $L_{eq} = \frac{1}{n}(L_r + L_s')$. Therefore, $T_{req} = \frac{L_{eq}}{R_{eq}} = T$.

This result shows that the response time of each motor is equal to the time constant of a single motor after the multi-motor system is disturbed. It can be concluded that when any of the motors constituting the ring network control system is disturbed, there is no time delay between the motors.

VI. EXPERIMENTAL SIMULATION

To verify the effect of CRCF on multi-motor coordinated control, the control performance of the control strategy was quantitatively analyzed by MATLAB. Furthermore, the real-time effect of the CRCF control strategy is qualitatively

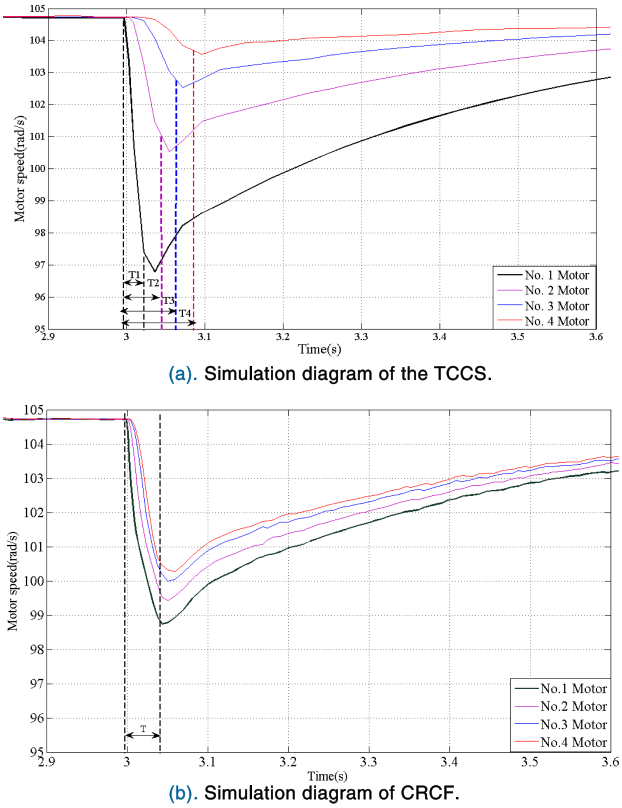

FIGURE 13. (a) Simulation diagram of the TCCS. (b) Simulation diagram of CRCF.

TABLE 2. Parameter value of the motors.

P(kW)	37	$J_D(kg \cdot m^2)$	0.41
R(Ω)	0.18	P_N	2
T_l (S)	0.0089	k_s (S)	110
k_T (S)	6.06	λ	30/3.14
τ_n	0.445	K_N	151.5

analyzed by the RT-LAB real-time simulation platform. The parameters of the motors are shown in Table 2.

The closed-loop transfer function of the AC asynchronous motor drive unit is shown as follows:

$$G(2) = \frac{\omega}{V} = \frac{7.1S + 15.86}{0.0089S^3 + S^2 + 67.4S + 151.1} \quad (45)$$

The three characteristic roots are $\lambda_1 = -2.32$, $\lambda_2 = -54.8 + 65.7i$, $\lambda_3 = -54.8 - 65.7i$. The corresponding eigenvector matrix and its inverse matrix are obtained by the equation as shown at the bottom of next page,

Then, the impulse response matrix (46), as shown at the bottom of the next page. where e^{At} is bounded and $\lim_{t\to\infty} e^{At} = 0$, and all the elements of the impulse response matrix $H(t)$ satisfy $\int_0^\infty |h(t)|dt < \infty$; therefore, the system has external stability.

Under the external stability of the system and the condition that the system is fully controllable and observable,

the system is also internally stable; therefore, the system is stable.

A. MATLAB/SIMULINK EXPERIMENTAL VERIFICATION

The CRCF model of four-motor coordinated control is established, and the effectiveness of the proposed CRCF is demonstrated by comparing with the TCCS in the MATLAB simulation experiment. The experiments are conducted with a velocity ratio of 1:1:1:1 and a velocity ratio of 4:3:2:1.

1) SPEED RATIO IS 1:1:1:1

The rated speed of the four asynchronous motors is *1,000 r/min*, and the stable running angular velocity is *104.7 (rad/s)*. After the four motors reach stable operation, a torque of 100 *N·m* is applied to the No. 1 motor. The four-motor output speed simulation waveforms are shown in Fig. 13(a) using the TCCS and in Fig. 13(b) using CRCF.

The waveform comparison in Fig. 13(a) it can be seen that there is a lag in the motor speed following in the TCCS control strategy; the further the distance from the disturbed motor, the longer the lag time. The response time of the fourth motor is approximately 4 times that of the first motor; $T_4 \approx 4T_1$. However, there is almost no lag in Fig. 13(b) using the CRCF control strategy proposed in this paper; the response times of the four motors are basically synchronized; $T_4 \approx T_3 \approx T_2 \approx T_1 = T$. Moreover, it can also be seen from Table 3 that when the CRCF is adopted, the overshoot of the first motor is greatly reduced, and the overshoot of the other motors is close to that of the first motor. It is proved that the CRCF has stronger ability to follow and coordinate among multi-motor compared with the TCCS control strategy, improves the control accuracy of the system, and prevents possible damage to each motor caused by additional mechanical torque due to excessive speed differences.

The waveform comparison in Fig. 13(a) and Fig. 13(b) shows that when the system is subjected to load disturbance, the CRCF control strategy makes the speed following ability of each motor better, the overshoot smaller, the adjustment time shorter, and the coordinated control stronger.

TABLE 3. Overshoot comparison under synchronous operation.

Motor sequence	No. 1	No. 2	No. 3	No. 4
TCCS	7.5%	3.7%	1.9%	0.7%
CRCF	5.5%	4.9%	4.5%	4%

TABLE 4. Overshoot calculation under proportional speed operation.

Motor sequence	No. 1	No. 2	No. 3	No. 4
TCCS	17%	2.6%	2.0%	1.9%
CRCF	14%	10%	9.6%	7.7%

The overshoot percentage calculation results are shown in Table 3. The overshoot of the disturbed motor (No.1) using CRCF is smaller than that obtained by using the TCCS.

2) SPEED RATIO OF 4:3:2:1

When four AC asynchronous motors run at a 4:3:2:1 speed ratio, their speeds are *1,000 r/min, 750 r/min*, *500 r/min, 250 r/min*, and their angular velocities are *104.7 (rad/s), 78.5 (rad/s), 52.33 (rad/s), 26.17 (rad/s)*, respectively. A torque of 100 *N·m* is applied to the No. 1 motor. The output speed waveforms of the four motors are shown in Fig. 14(a) using the TCCS and in Fig. 14(b) using CRCF.

It can be seen from Fig. 14(a) and Fig. 14(b) that the time for the speed of the four motors to return to the rated speed after disturbance is shorter when using CRCF than when using the TCCS. Moreover, the speed following ability of each motor is better, the overshoot of the disturbed motor (No. 1) is smaller, the adjustment time is shorter, and the coordination is stronger. The overshoot percentage calculation results are shown in Table 4. The motor overshoot of the TCCS is obviously larger than that of CRCF, and the following ability is weaker compared to that of CRCF.

It can be concluded that when the motor is running at a certain speed ratio, once one of the motors is disturbed, other motors will make corresponding speed changes faster when using CRCF than when using the TCCS. CRCF reduces the overshoot of the disturbed motor and effectively eliminates lag. Therefore, the CRCF control strategy can be

$$p = \begin{bmatrix} 0.16 & 2.43\times10^{-5} - 0.0001i & 2.43\times10^{-5} + 0.0001i \\ -0.39 & 0.007 + 0.009i & 0.007 - 0.009i \\ 0.91 & -0.99 & 0.99 \end{bmatrix}$$

$$p^{-1} = \begin{bmatrix} 6.18 + 8.88\times10^{-16}i & 0.09 + 3.82\times10^{-16}i & 0.0008 - 1.31\times10^{-19}i \\ 2.78 - 131.85i & 0.042 - 57.71i & -0.50 - 0.44i \\ 2.78 + 131.85i & 0.042 + 57.71i & -0.50 + 0.44i \end{bmatrix}$$

$$\begin{aligned} H(t) &= \begin{bmatrix} b_0 & b_1 & 0 \end{bmatrix} p \begin{bmatrix} e^{-\lambda_1 t} & & \\ & e^{-\lambda_2 t} & \\ & & e^{-\lambda_3 t} \end{bmatrix} p^{-1} \begin{bmatrix} 0 \\ 0 \\ 1 \end{bmatrix} = \begin{bmatrix} b_0 & b_1 & 0 \end{bmatrix} p \begin{bmatrix} e^{-2.32t} & & \\ & e^{(-54.8+65.7i)t} & \\ & & e^{(-54.8-65.7)t} \end{bmatrix} p^{-1} \begin{bmatrix} 0 \\ 0 \\ 1 \end{bmatrix} \\ &= e^{-2.32t}(0.16b_0 - 0.39b_1) + e^{(-54.8+65.7i)}(-0.5 - 0.44i)\left[b_0(2.43\times10^{-5} - 0.001i) + b_1(0.007 + 0.009i)\right] \\ &\quad + e^{(-54.8-65.7i)}(-0.5 + 0.44i)\left[b_0(2.43\times10^{-5} + 0.001i) + b_1(0.007 - 0.009i)\right] \end{aligned} \tag{46}$$

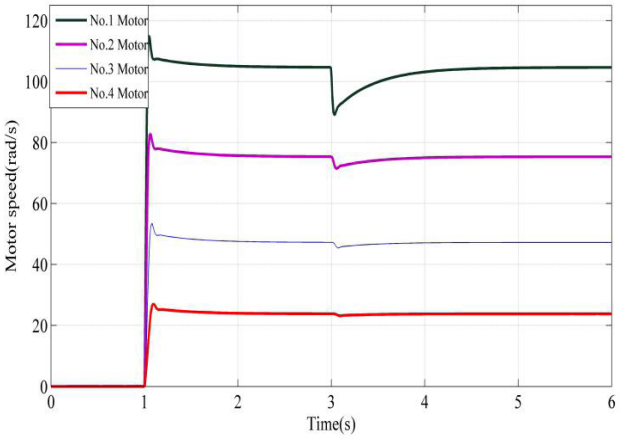

(a). Simulation diagram of the TCCS.

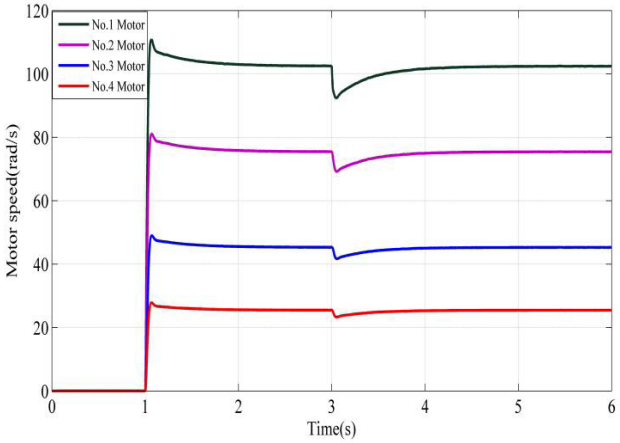

(b). Simulation diagram of CRCF.

FIGURE 14. (a) Simulation diagram of the TCCS. (b) Simulation diagram of CRCF.

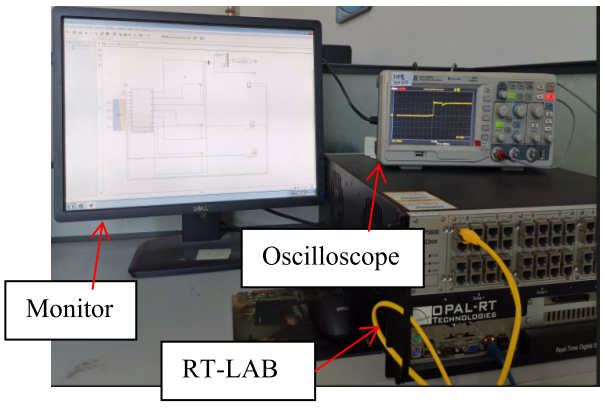

FIGURE 15. Real-time simulation.

widely applied to robot control equipment, which has higher-precision requirements.

B. RT-LAB EXPERIMENTAL VERIFICATION

To further verify the actual coordinated control effect of CRCF, a real-time simulation experiment is executed on the RT-LAB real-time simulation platform to observe the speed waveform through the oscilloscope.

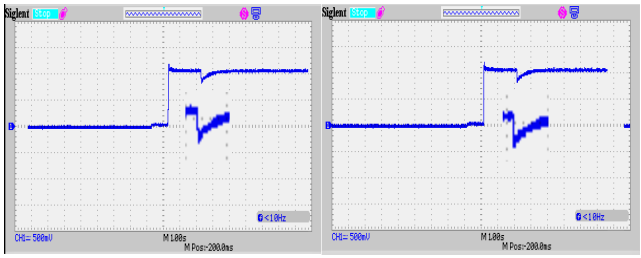

(a). No. 1 motor speed tracking comparison.

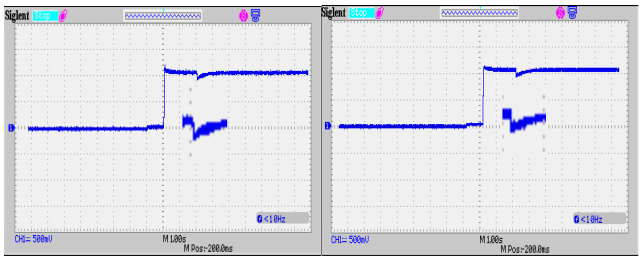

(b). No. 2 motor speed tracking comparison.

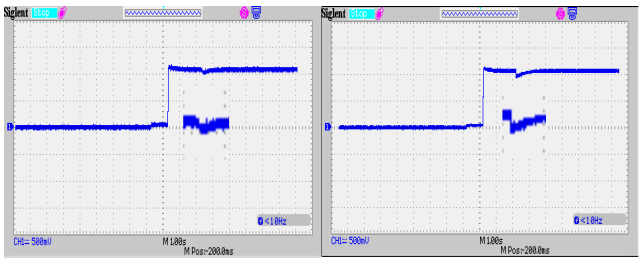

(c). No. 3 motor speed tracking comparison.

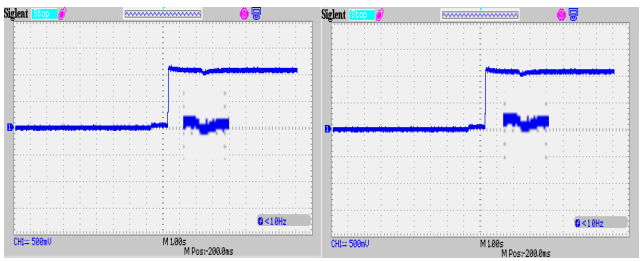

(d). No. 4 motor speed tracking comparison.

FIGURE 16. (a) No. 1 motor speed tracking comparison. (b) No. 2 motor speed tracking comparison. (c) No. 3 motor speed tracking comparison. (d) No. 4 motor speed tracking comparison.

The comparison results of multi-motor speed synchronization experiments using the TCCS method and CRCF method are shown in Fig. 16. The images on the left in the panels of Fig. 16 show the simulation results for the TCCS, and the images on the right of the panels of Fig. 16 show the simulation results for CRCF.

Through the comparison in Fig. 16, it can be seen that the speed tracking between adjacent motors is weak using the TCCS, and the lag of speed tracking is obvious. However, using CRCF, the speed tracking is improved for the No. 2 motor and the No. 3 motor, and there is almost no lag. The motor speed overshoot ratio of CRCF is smaller than that of the TCCS, which indicates that the CRCF method makes the speed changes of the motors more consistent, the

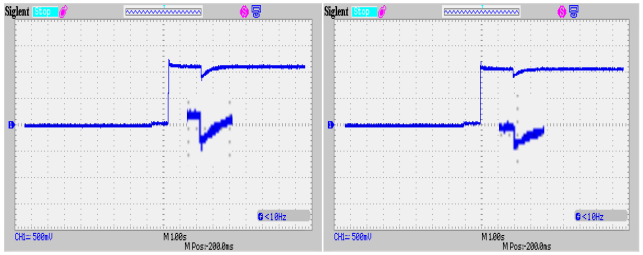

(a). No. 1 motor speed tracking comparison.

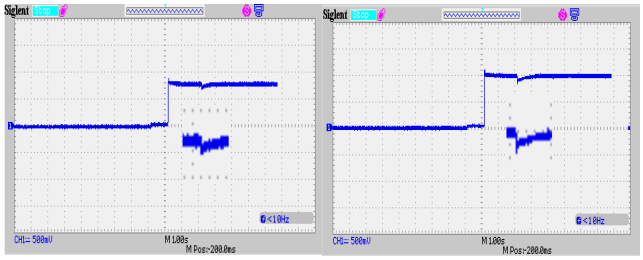

(b). No. 2 motor speed tracking comparison.

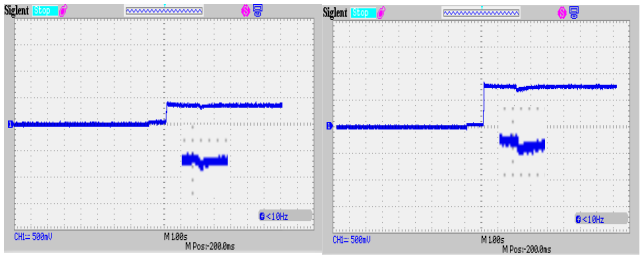

(c). No. 3 motor speed tracking comparison.

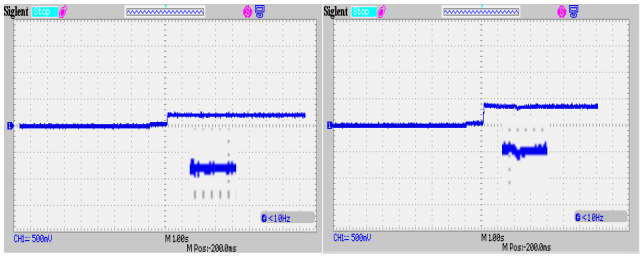

(d). No. 4 motor speed tracking comparison.

FIGURE 17. (a) No. 1 motor speed tracking comparison. (b) No. 2 motor speed tracking comparison. (c) No. 3 motor speed tracking comparison. (d) No. 4 motor speed tracking comparison.

speed tracking is better and the coordination between motors is stronger.

The experimental results of the motor speed proportionally compared with the TCCS and CRCF are shown in Fig. 19 when the motors are running at a special speed ratio of 4:3:2:1. The images on the left in the panels of Fig. 17 show the experimental results of the TCCS, and the images on the right of the panels in Fig. 17 show the experimental results of CRCF.

It can be seen from Fig. 17 that the speed following ability of the TCCS is gradually weakened, and the No. 4 motor has essentially no speed following. However, when using

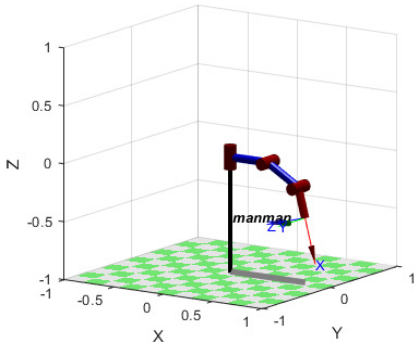

FIGURE 18. Simulation diagram of the robot arm.

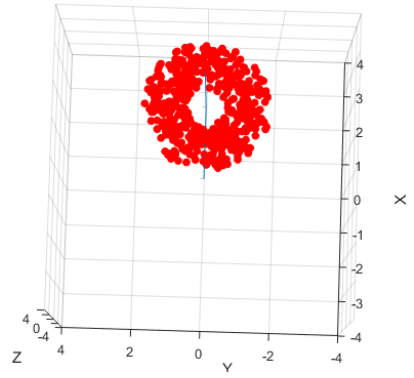

FIGURE 19. The working space mapping diagram of the robotic arm.

the CRCF control strategy the speed following ability is improved significantly; the overshoot ratio of the motors is much smaller. No lag between motors using CRCF, real-time response is stronger.

The results of the above experiments show that CRCF achieves a remarkable control effect to maintain the stability of multi-motor synchronous operation. It also proves that CRCF has obvious effects on coordination control performance in a multi-motor system due to strong speed tracking and anti-interference ability. Therefore, it has a wider range of applications.

C. SIMULATION ANALYSIS OF A MANIPULATOR WORKSPACE

The three-dimensional working space of a robot driven by multi-motor is the sum of the space points that the end actuator can reach. Except for the drive motor of the end -actuator, each motor drives a joint. The working space size of the robot arm determines the motion range of the robot. Therefore, an important indicator for measuring the working capacity of the robot is its working space. Given a value for each arm length, the kinematics model of the robotic arm is established using MATLAB, as shown in Fig. 18. The working space map of the robot arm is obtained.

Based on the Monte Carlo method, the working space of the robotic arm is drawn using MATLAB. When the robotic arms take $L_1 = 381\,mm$, $L_2 = 356\,mm$ and $L_3 = 263\,mm$ in Fig. 1, the trajectory of the robotic arm is an elliptical

cylinder. At a certain time, the working space that the robotic arm can reach is mapped to the *xoy* plane, as shown in Fig. 19.

VII. CONCLUSION

The CRCF method proposed in this paper effectively improves the coordinated control ability of multiple motors. Its fuzzy control can perform real-time speed error compensation, which further improves the follow-up ability between motor speeds. Its loop network control structure eliminates the problem of feedback lag compared with master-slave non-ring control, further improving the speed tracking accuracy between motors. Comparative test results show that the follow-up ability and the overshoot of the proposed method are better than those of the traditional non-ring network master-slave methods. The overshoot of the proposed method is smaller, the stabilization time is shorter, and the anti-interference ability is stronger. However, this control strategy is currently only a semi-physical simulation. The feasibility of practical applications needs further verification. The next step is to apply this control strategy to the coordinated control of robot motors and to study how to achieve multi-objective coordinated control of multiple motors, such as torque, speed, and position control, thus allowing the verification of the feasibility of its practical engineering application.

REFERENCES

[1] J.-S. Zhao, F.-L. Chu, and Z.-J. Feng, "Kinematics of spatial parallel manipulators with tetrahedron coordinates," *IEEE Trans. Robot.*, vol. 30, no. 1, pp. 233–243, Feb. 2014.

[2] D. Corinaldi, L. Carbonari, and M. Callegari, "Optimal motion planning for fast pointing tasks with spherical parallel manipulators," *IEEE Robot. Autom. Lett.*, vol. 3, no. 2, pp. 735–741, Apr. 2018.

[3] R. D. Valentine, J. G. Trasky, and D. R. Rippin, "Load sharing of dual motor grinding mill drives," *IEEE Trans. Ind. Appl.*, vol. IA-13, no. 2, pp. 161–168, Mar. 1977.

[4] Z.-D. Wang, K.-J. Li, J.-G. Ren, L.-J. Sun, J.-G. Zhao, Y.-L. Liang, W.-J. Lee, Z.-H. Ding, and Y. Sun, "A coordination control strategy of voltage-source-converter-based MTDC for offshore wind farms," *IEEE Trans. Ind. Appl.*, vol. 51, no. 4, pp. 2743–2752, Jul. 2015.

[5] A. Casavola, M. Papini, and G. Franze, "Supervision of networked dynamical systems undercoordination constraint," *IEEE Trans. Robot. Automat.*, vol. 51, no. 3, pp. 421–437, Mar. 2006.

[6] Y. Yang, C. Hua, and X. Guan, "Adaptive fuzzy finite-time coordination control for networked nonlinear bilateral teleoperation system," *IEEE Trans. Fuzzy Syst.*, vol. 22, no. 3, pp. 631–641, Jun. 2014.

[7] Y. Koren, A. Shani, and J. Ben-Uri, "Numerical control of a lathe," *IEEE Trans. Ind. Gen. Appl.*, vol. IGA-6, no. 2, pp. 175–179, Mar. 1970.

[8] L. Feng, Y. Koren, and J. Boreustein, "Cross-coupling motion controller for mobile robots," *IEEE Control Syst. Mag.*, vol. 13, no. 6, pp. 35–43, Dec. 1993.

[9] M. Tomizuka, J. S. Hu, and T. C. Chiu, "Synchronization of two motion control axes under adaptive feedforward control," *J. Dyn. Syst., Meas. Control*, vol. 11, no. 4, pp. 196–203, 1992.

[10] D. Sun and J. K. Mills, "Adaptive synchronized control for coordination of two robot manipulators," in *Proc. IEEE ICRA*, Washington, DC, USA, May 2002, pp. 976–981.

[11] D. Sun, G. Feng, C. M. Lam, and H. Dong, "Orientation control of a differential mobile robot through wheel synchronization," *IEEE/ASME Trans. Mechatronics*, vol. 10, no. 3, pp. 345–351, Jun. 2005.

[12] P. Saeedi, P. D. Lawrence, D. G. Lowe, P. Jacobsen, D. Kusalovic, K. Ardron, and P. H. Sorensen, "An autonomous excavator with vision-based track-slippage control," *IEEE Trans. Control Syst. Technol.*, vol. 13, no. 1, pp. 67–84, Jan. 2005.

[13] D. Sun, X. Shao, and G. Feng, "A model-free cross-coupled control for position synchronization of multi-axis motions: Theory and experiments," *IEEE Trans. Control Syst. Technol.*, vol. 15, no. 2, pp. 306–314, Mar. 2007.

[14] F.-J. Lin, P.-H. Chou, C.-S. Chen, and Y.-S. Lin, "DSP-based cross-coupled synchronous control for dual linear motors via intelligent complementary sliding mode control," *IEEE Trans. Ind. Electron.*, vol. 59, no. 2, pp. 1061–1073, Feb. 2012.

[15] M. H. Mohammadi and D. A. Lowther, "A computational study of efficiency map calculation for synchronous AC motor drives including cross-coupling and saturation effects," *IEEE Trans. Magn.*, vol. 53, no. 6, pp. 1–4, Jun. 2017.

[16] Y. Shi, J. Chai, X. Sun, and S. Mu, "Detailed description and analysis of the cross-coupling magnetic saturation on permanent magnet synchronous motor," *J. Eng.*, vol. 2018, no. 17, pp. 1855–1859, Nov. 2018.

[17] C.-S. Chen and L.-Y. Chen, "Robust cross-coupling synchronous control by shaping position commands in multiaxes system," *IEEE Trans. Ind. Electron.*, vol. 59, no. 12, pp. 4761–4773, Dec. 2012.

[18] Z. Wang, C. Hu, Y. Zhu, S. He, M. Zhang, and H. Mu, "Newton-ILC contouring error estimation and coordinated motion control for precision multiaxis systems with comparative experiments," *IEEE Trans. Ind. Electron.*, vol. 65, no. 2, pp. 1470–1480, Feb. 2018.

[19] Y. Lu, "Adaptive-fuzzy control compensation design for direct adaptive fuzzy control," *IEEE Trans. Fuzzy Syst.*, vol. 26, no. 6, pp. 3222–3231, Dec. 2018.

[20] J. Song, Y. Niu, J. Lam, and H.-K. Lam, "Fuzzy remote tracking control for randomly varying local nonlinear models under fading and missing measurements," *IEEE Trans. Fuzzy Syst.*, vol. 26, no. 3, pp. 1125–1137, Jun. 2018.

[21] J. Qiu, X. S. Ding, H. Gao, and S. Yin, "Fuzzy-model-based reliable static output feedback H_∞ control of nonlinear hyperbolic PDE systems," *IEEE Trans. Fuzzy syst.*, vol. 24, no. 2, pp. 388–400, Apr. 2016.

[22] H. Li, X. Sun, L. Wu, and H. K. Lam, "State and output feedback control of interval type-2 fuzzy systems with mismatched membership functions," *IEEE Trans. Fuzzy Syst.*, vol. 23, no. 6, pp. 1943–1957, Dec. 2015.

[23] X. Zeng, Y. Wang, D. Song, L. Zhu, G. Tian, and Z. Li, "Coordinated control algorithm of a dual motor for an electric variable transmission hybrid system," *IEEE Access*, vol. 6, pp. 35669–35682, 2018.

[24] H. Hou, X. Nian, H. Xiong, Z. Wang, and Z. Peng, "Robust decentralized coordinated control of a multimotor Web-winding system," *IEEE Trans. Control Syst. Technol.*, vol. 24, no. 4, pp. 1495–1503, Jul. 2016.

[25] L. P. Di Noia and R. Rizzo, "Design of a five-phase permanent-magnet motor for the electric steering of an aircraft nose landing gear," *IET Electr. Syst. Transp.*, vol. 7, no. 4, pp. 327–333, Dec. 2017.

[26] B. Zhang, J. Yuan, L. Qiu, N. Cheung, and J. F. Pan, "Distributed coordinated motion tracking of the linear switched reluctance machine-based group control system," *IEEE Trans. Ind. Electron.*, vol. 63, no. 3, pp. 1480–1489, Mar. 2016.

[27] J. Liao, Z. Chen, and B. Yao, "Model-based coordinated control of four-wheel independently driven skid steer mobile robot with wheel-ground interaction and wheel dynamics," *IEEE Trans Ind. Informat.*, vol. 15, no. 3, pp. 1742–1752, Mar. 2019.

[28] J. Liao, Z. Chen, and B. Yao, "Performance-oriented coordinated adaptive robust control for four-wheel independently driven skid steer mobile robot," *IEEE Access*, vol. 5, pp. 19048–19057, 2017.

[29] X. Yang, L. Zhang, W. Xie, and J. Zhang, "Sequential and iterative distributed model predictive control of multi-motor driving cutterhead system for TBM," *IEEE Access*, vol. 7, pp. 46977–46989, 2019.

[30] L. Chen, T. Chen, X. Xu, Y. Cai, H. Jiang, and X. Sun, "Multi-objective coordination control strategy of distributed drive electric vehicle by orientated tire force distribution method," *IEEE Access*, vol. 6, pp. 69559–69574, 2018.

[31] J. Wang, Z. Luo, Y. Wang, B. Yang, and F. Assadian, "Coordination control of differential drive assist steering and vehicle stability control for four-wheel-independent-drive EV," *IEEE Trans. Veh. Technol.*, vol. 67, no. 12, pp. 11453–11467, Dec. 2018.

[32] L. Sun, M. Cheng, H. Wen, and L. Song, "Motion control and performance evaluation of a magnetic-geared dual-rotor motor in hybrid powertrain," *IEEE Trans. Ind. Electron.*, vol. 64, no. 3, pp. 1863–1872, Mar. 2017.

[33] T. Shi, H. Liu, Q. Geng, and C. Xia, "Improved relative coupling control structure for multi-motor speed synchronous driving system," *IET Electr. Power Appl.*, vol. 10, no. 6, pp. 451–457, Jul. 2016.

[34] D. Zhang, G. Liu, H. Zhou, and W. Zhao, "Adaptive sliding mode fault-tolerant coordination control for four-wheel independently driven electric vehicles," *IEEE Trans. Ind. Electron.*, vol. 65, no. 11, pp. 9090–9100, Nov. 2018.

[35] Q. Shen, K. Dautenhahn, J. Saunders, and H. Kose, "Can real-time, adaptive human–robot motor coordination improve Humans' overall perception of a robot?" *IEEE Trans. Auton. Mental Develop.*, vol. 7, no. 1, pp. 52–64, Mar. 2015.
[36] L. Minati, M. Frasca, N. Yoshimura, and Y. Koike, "Versatile locomotion control of a hexapod robot using a hierarchical network of nonlinear oscillator circuits," *IEEE Access*, vol. 6, pp. 8042–8065, 2018.
[37] X. Jin, S. Wang, J. Qin, W. X. Zheng, and Y. Kang, "Adaptive fault-tolerant consensus for a class of uncertain nonlinear second-order multi-agent systems with circuit implementation," *IEEE Trans. Circuits Syst. I, Reg. Papers*, vol. 65, no. 7, pp. 2243–2255, Jul. 2018.
[38] X. Jin, C. Jiang, J. Qin, and W. X. Zheng, "Robust pinning constrained control and adaptive regulation of coupled Chua's circuit networks," *IEEE Trans. Circuits Syst. I, Reg. Papers*, vol. 66, no. 10, pp. 3928–3940, Oct. 2019.

YANJUAN WU received the M.S. degree in power systems and automation and the Ph.D. degree in power systems and automation from Tianjin University, Tianjin, China, in 2005 and 2013, respectively. She is currently an Associate Professor with the School of Electrical and Electronic Engineering, Tianjin University of Technology. Her current research interests include intelligent control, smart grids, and grid optimization and control.

YANBIN CHENG received the B.S. degree in electrical engineering and automation from the Zhengzhou Institute of Science and Technology, Zhengzhou, China, in 2017. He is currently pursuing the M.S. degree with the School of Electrical and Electronic Engineering, Tianjin University of Technology, Tianjin, China. His current research interests include fuzzy control and multimotor coordinated control.

YUNLIANG WANG received the M.S. degree in power systems and automation from Tianjin University, Tianjin, China, in 1988. He is currently a Professor with the School of Electrical and Electronic Engineering, Tianjin University of Technology. His current research interests include intelligent control, multimotor coordinated control, microcomputer control, and power electronics technology.